

NASA AG-GRANT

IN-92-CR

153008

P25

C S S A

THE RATIO OF MICROWAVES TO X-RAYS IN SOLAR FLARES
THE CASE FOR THE THICK TARGET MODEL

Edward T. Lu¹

and

Vahé Petrosian¹

CSSA-ASTRO-88-08

June 1988



CENTER FOR SPACE SCIENCE AND ASTROPHYSICS
STANFORD UNIVERSITY
Stanford, California

(NASA-CR-183102) THE RATIO OF MICROWAVES TO
X-RAYS IN SOLAR FLARES: THE CASE FOR THE
THICK TARGET MODEL (Stanford Univ-) 25 p

CSCI 03B

N88-26287

Unclas

G3/92 0153008

THE RATIO OF MICROWAVES TO X-RAYS IN SOLAR FLARES:
THE CASE FOR THE THICK TARGET MODEL

Edward T. Lu¹

and

Vahé Petrosian¹

CSSA-ASTRO-88-08

June 1988

¹also Department of Applied Physics, Stanford University

National Aeronautics and Space Administration Grant NSG 7092

National Science Foundation Grant ATM 8705084

The Ratio of X-rays to Microwaves in Solar Flares: The Case for the Thick Target Model

Abstract

We calculate the expected ratio of synchrotron microwave radiation to bremsstrahlung X-rays for thick target, thin target, and multithermal solar flare models. Our calculations take into account the variation of the microwave to X-ray ratio with X-ray spectral index. We compare the theoretical results with observed ratios of a sample of 51 solar flares with well known spectral index. From this we conclude that the nonthermal thick target model with a loop length of order 10^9 cm and magnetic field of 500 ± 200 G provides the best fit to the data. The thin target and multithermal models require unreasonably large density or pressure and/or low magnetic field to match the data.

I. Introduction

The similarity between the time profiles of the microwaves and X-rays from solar flares and the good correlation between their peak fluxes (see e.g. Cornell et al 1984, and Kai, Kosugi and Nitta 1985) are strong evidences that the two emissions are produced by the same or very a closely related population of electrons.

However, ever since the first simultaneous observations of microwaves and X-rays from solar flares (Peterson and Winckler 1959), there has been a controversy over the number of non-thermal electrons required to produce the X-ray and the microwave burst (see e.g. Takakura and Kai 1966; Holt and Ramaty 1969; Gary and Tang 1984). Several authors (Peterson and Winckler 1959; Schmahl, Kundu, and Dennis 1985) have claimed that the number of non-thermal electrons inferred from the X-ray burst is about $10^3 - 10^4$ times larger than the number of electrons needed for the production of the microwaves in a given flare. More recently, however, Gary (1985) and Kai (1986) show that the numbers of electrons deduced from the two emissions are the same.

Some of the discrepancy can be attributed to the neglect of self absorption of the synchrotron radiation (Holt and Ramaty 1969), when the comparison is carried out at low microwave frequency (< 10 GHz). This still leaves the picture unclear for optically thin synchrotron emission. The problem with using the optically thick flux is that it is very sensitive to the area and spatial geometry of the source. On the other hand, the microwave flux in the optically thin regime is sensitive to the total number of emitting electrons and less so to the geometry of the source. The optically thin microwave flux should therefore be a more reliable source of information when trying to determine whether or not a single population of electrons is responsible for both the microwaves and X-rays. In this optically thin case most of the claims of discrepancy can be attributed to the fact that earlier authors had calculated the electron population from the observed X-ray spectrum using the thin target bremsstrahlung model as opposed to the thick target model (Gary 1985).

The thin target model assumes that the high energy electrons responsible for the flare emit both bremsstrahlung X-rays and microwave synchrotron radiation in the same physical region. Thus, the same electron distribution is used for calculating both emissions. In a truly thin target

situation the mean free path of the electron is greater than the region where emission takes place, which is very unlikely.

It is now widely agreed that the accelerated electrons find themselves mostly on closed magnetic loops so that they are eventually stopped in the chromospheric plasma. If the electrons are accelerated at substantially high altitudes above the chromosphere, they essentially travel freely along the field lines in the corona. Once in or below the high density chromosphere they quickly (in a short distance) lose their energy. For the same reason most of the bremsstrahlung X-rays are also emitted from the latter region while the microwaves come primarily from coronal regions where the electrons spend most of their lifetime. This will not be true if the magnetic field increases as rapidly as the density below the chromosphere. This, however, is not believed to be the case. Thus, while the same electron population is responsible for both X-rays and microwaves, the emissions come from different physical regions. The microwaves are produced in the coronal portion of the loop by a spectrum of electrons which is essentially the same as that of the accelerated electrons, while X-rays originate in the chromosphere from the harder thick target electron spectrum.

Multithermal models have also been proposed to explain the hard X-ray emission from flares (Brown 1974, Dulk and Dennis 1982). Here the X-rays come from thermal bremsstrahlung from a multitemperature plasma with temperatures above 10^8 K. The microwave emission is then the sum of many thermal synchrotron spectra. Dulk and Dennis (1982) have used such a model to explain hard X-rays and the optically thick part of the microwave spectrum.

In this paper we compare the observed microwave and X-ray fluxes of flares with the theoretical expectations of the three models mentioned above in order to clarify the situation and set constraints on the model parameters such as plasma density, magnetic field and flaring loop sizes. We make this comparison for a statistical sample of flares instead of a single flare, which has been carried out frequently in the past. More importantly however, instead of just considering the correlation between X-ray and microwave fluxes, we consider the observed variation of the ratio of the fluxes with the X-ray spectral index, and compare this with the predictions of the models. It turns out that the inclusion of the spectral index information provides strong constraints because, as we shall

see, the ratio of the fluxes is a sensitive function of the spectral index.

The X-ray observations we use will be the peak fluxes and spectral indices of flares with a well defined power law spectra:

$$dJ_x(k) = \left(\frac{F_x(k_0)}{k_0^2} \right) (\gamma - 2)(k/k_0)^{-\gamma} dk \text{ photons s}^{-1}, \quad (1)$$

where k is the photon energy and $F_x(k_0)$ is the total photon energy flux above energy k_0 . Throughout this paper, all energies are given in units of $m_e c^2$ unless otherwise specified.

For each model, we invert the photon spectrum to obtain the spectrum of the bremsstrahlung radiating electrons. This inversion depends upon the angular distribution of the photons and the electrons. In the absence of knowledge of the spatial or angular distribution of the X-rays, we must assume an angular distribution for the radiating electrons. For $k_0 \ll 1$, the X-ray flux will be approximately isotropic. We will also assume that the electron distribution is isotropic. In general, a power law photon flux implies that the effective spectrum of the electrons is also a power law. Assuming the same spectrum extends to higher energies, we then calculate the expected optically thin synchrotron radiation at a specified frequency for each model and for various values of the magnetic field B . This extrapolation needs some scrutiny, especially for low values of B because the energy of the electrons producing the microwaves is much larger (possibly relativistic) than those (non-relativistic ones) producing the X-rays. We shall return to the observational evidence for or against this assumption and comment on its effects. Given the synchrotron flux $S(\nu)$, we then compute the dimensionless ratio

$$R(\gamma, B) = \frac{\nu S(\nu)}{F_x(k_0)}, \quad (2)$$

and compare it with observations.

In the next section we describe the three models and derive the electron spectrum for each model. Then in section III we derive the synchrotron spectrum $S(\nu)$ and the ratio R . Here we give some new formulae for synchrotron emission from semi-relativistic electrons. Finally, in section IV we compare the ratio R with that from 51 observed flares and discuss the implications of this comparison.

II. Electron Distributions

We believe, and it is widely accepted, that the most likely model for production of the power law impulsive X-ray flux of a flare is the non-thermal thick target model. The presence of the magnetic fields and their closed loop structures dictate this conclusion. Accelerated non-relativistic or semi-relativistic electrons in such a configuration will lose most of their energy via Coulomb collisions in the thick target high density chromosphere with a well-defined yield of bremsstrahlung X-rays. If the field lines are open to the interplanetary medium, electrons with pitch angles directed downward will behave as above. Those electrons directed outward will lose some energy due to collisions and radiate X-rays as in a thin target model, but escape with most of their energy and with their initial distribution intact. The thick target X-rays will be dominant unless the majority of the accelerated electrons are directed outward. This seems unlikely because i) it necessarily implies a much lower X-ray yield and much larger total energy for the accelerated electrons, and ii) the number of outgoing electrons observed directly near the Earth and that deduced from type III bursts is much less than those needed for production of the X-rays.

Nevertheless, in addition to the thick target model, we shall also consider the thin target model, primarily for the purpose of comparison with earlier works. Furthermore, we describe results for thermal models which, because of the power law spectrum of the X-rays, must be multi-temperature. We should note at the outset that because there are many parameters in the models, any model can be brought into agreement with observations with proper adjustment of these parameters. The question is then which set of required parameters are reasonable and acceptable based on other observations or theoretical arguments. As we shall see, the thick target model implies a more reasonable set of flare plasma parameters than the other two models.

We note here that most of the equations cited below are not new and have been in the literature for some time now. But for completeness we present them here with the briefest descriptions. We will assume the electrons are non-relativistic in describing the X-ray emission. This is an excellent approximation as long as we restrict ourselves to X-ray energies less than ~ 100 keV.

(a) Non-thermal Thick Target Models

Here we assume that the accelerated electrons are injected at the top of a symmetric coronal loop at a steady rate (i.e., for a time longer than their lifetime) with the flux

$$dJ_e(E) = \frac{F_e(E_0)(\delta' - 1)}{E_0^2} (E/E_0)^{-\delta'-1} dE \text{ s}^{-1}, \quad (3)$$

where $F_e(E_0)$ is the total energy flux of electrons with energy greater than E_0 .

For the purpose of calculation of spatially unresolved X-rays, it is unimportant where the X-rays are emitted. Following Petrosian (1973) we can write for the X-ray flux given in equation (1)

$$F_x(k_0) = F_e(E_0)Y(k_0), \quad (4)$$

where $Y(k_0)$ is the yield of X-rays with energies $> k_0$ by electrons with energies $> E_0$. In what follows we set $k_0 = E_0$. For the power law distribution of equation (3)

$$Y(E_0) = \frac{16}{3} \left(\frac{\alpha}{4\pi \ln \Lambda} \right) E_0 \left(\frac{2}{\delta'} \right)^2 \left(\frac{1}{\delta' - 2} \right), \quad (5)$$

where $\delta' = \gamma$ the photon spectral index, α is the fine structure constant and $\ln \Lambda \approx 22$ is the Coulomb logarithm (note that our $\ln \Lambda$ here is defined to be one half of the definition used in Petrosian 1973). From equations (4) and (5), we find

$$F_e(E_0) = \frac{3}{64} \left(\frac{4\pi \ln \Lambda}{\alpha} \right) (\gamma - 2) \gamma^2 E_0^{-1} F_x(E_0), \quad (6)$$

which along with equation (3) relates the electron spectrum to the observed spectral index γ and flux $F_x(E_0)$ of the X-rays.

Electrons of energy E lose most of their energy after they have traversed a column depth $N(E) = 5 \times 10^{22} (E^2/(E+1)) \text{ cm}^{-2}$ (see e.g. Leach and Petrosian 1981) and emit mainly X-rays of energy $k \lesssim E$. We are interested in particles with $E > E_0 = 25 \text{ keV}$ which penetrate column depths greater than of order 10^{20} cm^{-2} . If the column depth of the coronal portion of the loop (from the top of the loop to the transition region) $N_{tr} < 10^{20} \text{ cm}^{-2}$, most of the X-rays will be radiated below the transition region. More importantly, however, the microwave producing electrons will have much larger energy (even $E \gtrsim 1$ for low fields, see below) and therefore will be completely

unaffected by collisions in the corona. The spectrum of electrons above the transition region will then be given by

$$f(E)dE = \frac{L}{\beta c \bar{\mu}} dJ_e(E) = \left(\frac{3\pi L \ln \Lambda}{16\alpha c \bar{\mu}} \right) \frac{F_x(E_0)}{\beta E_0^3} (\gamma - 2)(\gamma - 1)\gamma^2 \left(\frac{E}{E_0} \right)^{-\gamma-1} dE, \quad (7)$$

where L is the length of the loop above the transition region and $\bar{\mu}$ is the average pitch angle throughout the loop. Below the transition region the flux of the non-thermal particles decreases quickly (within a few density scale heights H_n) because of the rapid increase in plasma density (see e.g., Leach and Petrosian 1981).

The synchrotron flux could be related to the injected electron flux by calculating the thick target synchrotron yield. This, however, requires a knowledge of the variation of magnetic field and density along the loop and the geometry of the loop. In the absence of such detailed information we make the approximation that the total synchrotron flux is due to the electrons in the coronal portion of the loop since the number of particles above the transition region will be far larger than the number of particles below the transition region. Because the flux of particles below the transition region is less than that above it, the synchrotron contribution from that region will be less by a factor of $\sim (H_n/L) \ll 1$. This assumes a uniform B field. Although the B field is expected to be higher in the chromosphere than in the corona, this increase is not sufficient to affect the above inequality. Also, for an isotropic electron distribution, the synchrotron emission is peaked in a direction perpendicular to the magnetic field and decreases to zero in the direction parallel to the magnetic field. For loops not situated near the solar limb, the angle between the line of sight and the local magnetic field, and therefore the microwave emissivity, is greatest at the top of the loop and smallest at the base of the loop. Consequently, we will ignore the synchrotron emission below the transition region and we use the distribution given in equation (7) to calculate the synchrotron emission from this model.

(b) Non-thermal Thin Target Models

In a thin target model the X-rays and microwaves are both produced by electrons of instantaneous energy spectrum $f(E)$. We will assume an isotropic electron momentum distribution. Using

the well known thin target formula (see e.g. Brown 1971, Lin and Hudson 1976) one can relate the electron spectrum to the observed X-ray spectrum of equation (1). However, we follow the same procedure used in Petrosian (1973, equation 29) to calculate the thick target spectrum since this approximation leads to a simpler analytic expression without loss of much accuracy. From this we find for the thin target case in the non-relativistic limit

$$f(E) = \frac{3\sqrt{2}}{64} \frac{(\gamma - 2)(\gamma - 1)\gamma}{\alpha r_0^2 c n_0} \frac{F_x(E_0)}{E_0^{3/2}} \left(\frac{E}{E_0} \right)^{-\gamma+1/2}, \quad (8)$$

where r_0 is the classical electron radius and n_0 is the background plasma density. In this model the same distribution of electrons also produces the microwave radiation via synchrotron emission in a magnetic field of strength B .

(c) Thermal Models

As mentioned above, a single temperature plasma does not give rise to a power law bremsstrahlung spectrum. However, as shown by Brown (1974), a multi-temperature plasma can produce a power law bremsstrahlung spectrum if the emission measure distribution $n^2(T_*)V(T_*)dT_*$ has a power law dependence on temperature parameter $T_* \equiv k_B T / m_e c^2$. Here n and V are the density and volume of a plasma element of temperature T and k_B is the Boltzmann constant. By integration of the thermal bremsstrahlung spectrum over all temperature it can be shown that the X-ray spectrum of equation (1) can be produced by an emission measure distribution

$$n^2(T_*)V(T_*) = \frac{3\sqrt{6}}{32\sqrt{\pi}} \frac{1}{\alpha c r_0^2} \frac{(\gamma - 2)}{\Gamma(\gamma - 1)} \frac{F_x(E_0)}{E_0^{3/2}} \left(\frac{T_*}{E_0} \right)^{-\gamma+1/2}, \quad (9)$$

where Γ is the gamma function. The total electron energy spectrum is then the sum of many Maxwell-Boltzmann distributions weighted by the product nV .

$$f(E) = \frac{2}{\sqrt{\pi}} E^{1/2} \int_0^\infty T_*^{-3/2} e^{-E/T_*} n(T_*)V(T_*)dT_* \quad (10)$$

It is clear that some additional assumption is needed in order to relate the electron distribution to the observed X-ray spectrum. Two common assumptions are constant pressure $n(T_*) = n_0 E_0 / T_*$ (Brown 1974) or constant density $n(T_*) = n_0$ (Dulk and Dennis 1982). Note that in the constant

pressure case n_0 is the density at temperature $T_* = E_0$. From equations (9) and (10) we then obtain

$$f(E) = \frac{3\sqrt{6}}{16\pi} \left(\frac{\gamma - 2}{\alpha c r_0^2 n_0} \right) \frac{\Gamma(\gamma - 1/2 \pm 1/2)}{\Gamma(\gamma - 1)} \frac{F_x(E_0)}{E_0^{3/2}} \left(\frac{E}{E_0} \right)^{-(\gamma - 1 \pm 1/2)}, \quad (11)$$

with the (+) sign for the constant density case and the (−) sign for the constant pressure case.

In summary, the total electron distribution inferred from the X-ray spectrum of equation (1) in the three models can be written as

$$f(E) = \left(\frac{3\pi}{16\sqrt{2}} \right) \left(\frac{1}{\alpha c} \right) \left(\frac{F_x(E_0)}{E_0^{7/2}} \right) h(\gamma) \left(\frac{E}{E_0} \right)^{-\delta}, \quad (12)$$

where

$$\delta = \begin{cases} \gamma + 3/2 & \text{thick target} \\ \gamma - 1/2 & \text{thin target} \\ \gamma - 1 \pm 1/2 & \text{thermal} \end{cases} \quad (13)$$

and

$$h(\gamma) = \begin{cases} \left(\frac{L \ln A}{\mu} \right) (\gamma - 2)(\gamma - 1)\gamma^2 & \text{thick target} \\ \left(\frac{1}{\pi} \right) \left(\frac{1}{n_0 r_0^2} \right) E_0^2 (\gamma - 2)(\gamma - 1)\gamma & \text{thin target} \\ \left(\frac{2\sqrt{3}}{\pi^2} \right) \left(\frac{1}{n_0 r_0^2} \right) E_0^2 \frac{\Gamma(\gamma - 1/2 \pm 1/2)}{\Gamma(\gamma - 1)} (\gamma - 2) & \text{thermal} \end{cases} \quad (14)$$

Note that for the thick target case we have used the non-relativistic approximation $\beta = (2E)^{1/2}$. We will discuss the validity of this and other approximations in the next sections when we calculate the expected microwave emission from these models and compare them with observations.

III. Microwave Emission

In evaluating the microwave spectrum the non-relativistic assumptions used so far are no longer applicable. The simple and well known ultra-relativistic synchrotron emissivity formula are also not accurate for the semi-relativistic regime we are concerned with here. We will make use of expressions derived by Petrosian (1981) for these energy ranges. In this paper various approximate expressions with varied complexity and accuracy are given for the synchrotron emissivity. These approximations are valid for high harmonics, i.e. at frequencies $\nu \gg \nu_b = eB/2\pi m_e c$. The most accurate result is obtained when the integration over the particle energies equation (P.8) is carried out numerically (equations preceded by P refer to Petrosian 1981). We have compared the results

of this integration with the detailed numerical evaluations using the sums over Bessel functions (cf. e.g. Bekefi 1966). We find excellent agreement.

This integration can also be carried out analytically using the method of steepest descent, leading to equation (P.11). This expression requires the solution of a transcendental equation and is too complicated for our purposes here. However, for $\nu \gg \nu_b$ an approximation similar to the ultra-relativistic approximation is possible. With this approximation, the synchrotron emissivity in $m_e c^2 \text{ s}^{-1} \text{ Hz}^{-1}$ from an isotropic electron distribution $f(E)$ is given by

$$S(\nu) = \left(\frac{2\pi^2 r_0 \nu_b}{c} \right) \left(\frac{\nu \sin \theta}{\nu_b} \right)^{1/2} f(E_1) X \exp[d \ln(f/\gamma) / d \ln \gamma^2 |_{\gamma=E_1+1}] \quad (15)$$

where θ is the angle between the magnetic field and the line of sight, $\gamma = E + 1$ is the Lorentz factor, and E_1 is the energy of the electrons with the largest contribution to the emission at frequency ν . The function X depends on the electron distribution and the harmonic number, but for the power law distribution we will consider, it takes on a particularly simple form. Equation (P.34) evaluates this for a power law electron spectrum of spectral index δ in the limit of high harmonics and relativistic electrons. It however does not yield a very accurate expression at moderate harmonics, especially for steep spectra ($\delta \gtrsim 5$) which are encountered in the present work. The principle error introduced in equation (P.34) is in assuming that $(\gamma_1 - 1) = E_1 \gg 1$ when substituting into equation (15). We have found that simply by not making this assumption when substituting into $f(E_1)$ in equation (15) but otherwise using (P.34), we obtain surprisingly good results in this intermediate regime. We therefore set

$$\gamma_1^2 = \frac{4\nu}{3\nu_b \delta \sin \theta} \text{ and, } X = (1 + \delta)^{-1/2}, \quad (16)$$

in which case we find for the power law electron distribution of equation (12)

$$S(\nu) = \left(\frac{2\pi^2 r_0 \nu_b \sin \theta}{c} \right) \left(\frac{\nu}{\nu_b \sin \theta (\delta + 1)} \right)^{1/2} \exp \left(-\frac{\delta + 1}{2} \right) f(E_1). \quad (17)$$

Figure 1 shows a comparison of this expression with the numerically integrated emissivity equation (P.8). As can be seen this provides a satisfactory approximation. However, for steep spectra and at large B field such that $\nu/\nu_b \delta$ approaches unity, this approximation overestimates

the emissivity. Because many authors have used and continue to use the empirical fits to the synchrotron emissivity by Dulk and Marsh (1982) we also plot the ratio of their expression to the numerical values. It is evident that even though their empirical expression provides a satisfactory approximation within the range of parameters tested by them, outside this range at low ν/ν_b and steep spectra it diverges away from the correct value faster than our result. The main purpose of figure (1) is to indicate that caution is needed when using either the simplest analytic formula of Petrosian or the empirical fits of Dulk and Marsh (1982).

Now finally the ratio R as defined in equation (2) becomes

$$R = \left(\frac{3\pi^3 r_0 \nu_b^2 \sin^2 \theta (\delta + 1)}{8\sqrt{2} \alpha c^2 E_0^{7/2}} \right) \left(\frac{\nu}{\nu_b \sin \theta (\delta + 1)} \right)^{3/2} h(\gamma) \exp \left(-\frac{\delta + 1}{2} \right) \left(\frac{E_1}{E_0} \right)^{-\delta}, \quad (18)$$

where $h(\gamma)$ and δ are given by equations (13) and (14) and

$$E_1 = \left(\frac{4\nu}{3\nu_b \delta \sin \theta} \right)^{1/2} - 1 = 9.0 \left(\frac{\nu}{17 \text{ GHz}} \right)^{1/2} \left[\left(\frac{B}{100 \text{ G}} \right) \delta \sin \theta \right]^{-1/2} - 1. \quad (19)$$

IV. Comparison With Observations And Conclusions

We have analyzed a sample of 53 flares with observations in both hard X-rays and microwaves for which the X-ray spectral index is known. The flares were observed in X-rays by the Hard X-ray Burst Spectrometer (HXBRS) aboard the *SMM* satellite (Dennis et al 1985). From the HXBRS observations we obtain the integrated hard X-ray flux $F_x(25 \text{ keV})$ above 25 keV, and the photon spectral index γ (which were kindly provided by Brian Dennis). The microwave observations were made at 17 GHz by Nobeyama observatory (Kosugi and Shiomi 1983). These flares are all the flares for which we had the X-ray spectral index and which also appeared in the listing of microwave flares observed at Nobeyama. This data is summarized in Table 1. Included in this table is the *SMM* flare number, the integrated X-ray flux $F_x(25 \text{ keV})$ in $\text{ergs s}^{-1} \text{ cm}^{-2}$, the microwave flux $S(17 \text{ GHz})$ in $\text{SFU} = 10^{-19} \text{ ergs s}^{-1} \text{ cm}^{-2} \text{ Hz}^{-1}$, the duration of the flare in X-rays and microwaves in seconds, and the value of the ratio R . We have plotted the ratio R for these flares versus the spectral index γ in figure 2. We have excluded from this and following figures two of the flares with very steep spectra ($\gamma > 9$) such that a power law spectrum is questionable. On the same graph we have

plotted the theoretical curves of R for magnetic field strengths of 350, 450, 550, and 650 G for the nonthermal thick target model with a loop length $L = 2 \times 10^9$ cm at a viewing angle of $\theta = 70^\circ$. We have assumed isotropic injection in the downward hemisphere so that $\bar{\mu} = 0.5$. From VLA imaging observations (Schmahl, Kundu, and Dennis 1985) and from theoretical arguments (Lu and Petrosian 1988), a loop length of order 10^9 cm is a reasonable value for L . As can be seen, the thick target model explains the data very well with these parameters for a small range of magnetic field strengths between 350 and 650 Gauss. Note though that the data could also be explained with a single value of magnetic field (~ 550 G) but with varying loop length and viewing angle.

For comparison, in figure 2 we have also plotted R where we have numerically integrated equation (P.8) for the distribution given in equation (7). Note that R actually increases with γ at large γ and large B . This is because for very steep spectra the X-ray yield decreases rapidly with γ since many of the bremsstrahlung photons will be emitted at energies below E_0 . On the other hand for large δ and B , the synchrotron emissivity becomes less dependent upon δ because more of the emission comes from lower harmonics.

We will now examine the accuracy of some of the assumptions used in calculating equation (18) for the thick target case. We replaced a factor of β in equation (7) by $(2E)^{1/2}$ when calculating the electron distribution in the loop. Thus we underestimate the value of R in equation (18) when the characteristic energy of the microwave emitting electrons E_1 becomes relativistic. As is evident from equation (19), the value of E_1 increases with decreasing B and γ ; $E_1 \approx 1.3$ at $B = 400$ G and $\gamma = 3$. We therefore make an error of a factor of ~ 1.5 in β . As can be seen in figure 2, the analytic expression underestimates R at low values of spectral index. This error however, decreases for larger B and steeper spectra.

At steeper spectra, the error is due to the analytic approximation to the synchrotron emissivity we have used. As can be seen from figure 1 and figure 2, our approximation overestimates the emissivity at large B and steep spectra. At 650 G and $\delta = 8$, corresponding to $\gamma = 6.5$, the analytic expression is too large by a factor of 4. However, for our purposes the analytic expression will suffice. As can be seen from figure 2, the analytic expression equation (18) provides a satisfactory

approximation to R . The errors introduced are within the uncertainties associated with the loop length, the viewing angle, and the magnetic field.

In figure (3), along with the same observations we show the theoretical values of R for the thin target case with density $n_0 = 10^{11} \text{ cm}^{-3}$. The curves of R for the multithermal constant density case are almost identical to those of the thin target case. This is because the thin target model and the multithermal constant density model both describe the same physical situation. Both models have a population of electrons emitting bremsstrahlung radiation in a constant density plasma. Not surprisingly then they result in similar values for R . The slight difference in the two expressions is due to approximations made in integrating over the bremsstrahlung cross section in the calculation of the thin target X-ray spectrum. As can be seen, a large range of magnetic field strengths is required, ranging from less than 50 G to more than 400 G. Thus the field strengths must vary by an order of magnitude in order to match the observations. A problem with this is the lack of flares with extremely high (> 10), or extremely low ($< 10^{-3}$) values of R which would be expected for flares with high field and flat spectra or for flares with low field and steep spectra. Another serious problem is the high density which must be assumed in order to match the observations. The thin target assumption breaks down for $n_0 = 10^{11} \text{ cm}^{-3}$ for source size of order 10^9 cm . A more realistic density would be of order 10^9 cm^{-3} , but this would lead to very large values of R which would be inconsistent with the observations, as earlier authors had found.

In figure (4) we plot R for the multithermal constant pressure model with $n_0 = nT_*/E_0 = 3.44 \times 10^{10} \text{ cm}^{-3}$. This corresponds to a gas pressure of $1.38 \times 10^3 \text{ dynes cm}^{-2}$. Again, as in the thin target case, a large range of magnetic fields is required to match the observations. The constant pressure multithermal model however leads to even higher values of R than the thin target model for reasonable parameters. Note that a magnetic field of order 200 G is needed in order to magnetically confine such a plasma. Clearly there is a problem since the predicted field strength for some flares is less than 50 G.

Finally, it must be stressed again that these results have assumed that the power law spectrum observed in X-rays extends to higher energies. There is some evidence from observations of gamma-

rays (photon energies from 300 keV to 1 MeV) that the electron spectrum flattens at higher energies (Vestrand et al 1987). Schmahl, Kundu, and Dennis (1985) also report observations of a flare which has an X-ray photon spectral index $\gamma = 4$ corresponding to a thick target $\delta = 5.5$. However, from the microwave spectrum they obtain an electron spectral index for this flare of $\delta \approx 3$. From their analysis of the optically thick microwaves they conclude that the electron spectrum drops off sharply at ~ 150 keV before flattening out to $\delta = 3$ at much higher energy. Thus, the assumption of a single power law electron spectrum may be suspect. If the spectrum does flatten such that there are more electrons at high energies than expected from the X-ray observations, the value of magnetic field required to match the observations decreases. This is acceptable for the thick target model but presents a further problem for the thin target and thermal models. However as pointed out above, for the thick target model the value of the critical energy E_1 rarely exceeds 500 keV. Thus, the above mentioned changes in the electron spectral index will not have a large effect so that the thick target result remains accurate to the degree discussed earlier.

Thus we conclude that the observed microwave to X-ray ratios of solar flares are consistent with a single population of electrons producing both emissions. The thick target model with a reasonable set of flare parameters ($350 \text{ G} \lesssim B \lesssim 650 \text{ G}$ and $L \approx 2 \times 10^9 \text{ cm}$) explains the data quite well. The thin target and thermal models, however, have more difficulty in explaining the observations. A more rigid criteria for inclusion of flares in the sample such as limiting it to short, impulsive flares may lead to a smaller dispersion in parameters. In further work, we intend to study the temporal evolution of R versus γ for single flares, which could lead to stronger constraints on flare parameters.

Acknowledgements: We would like to thank Brian Dennis for supplying the X-ray spectral data. We would also like to thank Russell Hamilton and James McTiernan for helpful discussions and Marc Goldburg for computer help. This work was supported by NASA grant NSG7092 and NSF grant ATM8705084.

Table 1: Flare X-ray and Microwave Data

Flare	$F_x(25\text{ keV})$	$S(\nu)$ (SFU)	γ	t_x	t_μ	R
40	1.2×10^{-5}	145	4.4	145	> 120	2.09×10^{-2}
58	1.3×10^{-6}	53	3.3	400	300	6.94×10^{-2}
77	8.3×10^{-6}	203	3.4	500	90	4.15×10^{-2}
85	1.0×10^{-6}	49	4.5	160	120	8.33×10^{-2}
127	5.4×10^{-6}	330	3.9	960	3300	1.04×10^{-1}
150	6.1×10^{-6}	208	4.4	2100	300	5.80×10^{-2}
160	5.5×10^{-7}	42	3.8	30	36	1.30×10^{-1}
165	5.1×10^{-6}	73	8.0	100	4200	2.43×10^{-2}
187	1.3×10^{-5}	45	6.9	1525	630	5.88×10^{-3}
261	1.6×10^{-6}	19	6.0	990	84	2.02×10^{-2}
386	5.0×10^{-7}	36	4.0	150	30	1.22×10^{-1}
428	6.9×10^{-6}	36	5.7	190	600	8.87×10^{-3}
458	8.4×10^{-6}	168	2.7	470	78	3.40×10^{-2}
466	1.1×10^{-5}	124	4.8	385	396	1.92×10^{-2}
479	3.1×10^{-5}	275	4.3	635	156	1.51×10^{-2}
634	9.2×10^{-5}	940	4.2	279	252	1.73×10^{-2}
651	5.6×10^{-7}	28	5.3	50	120	8.50×10^{-2}
679	7.7×10^{-6}	51	3.2	93	36	1.13×10^{-2}
683	2.6×10^{-5}	549	3.4	368	210	3.59×10^{-2}
688	1.2×10^{-4}	953	2.8	691	330	1.35×10^{-2}
716	5.0×10^{-6}	33	5.4	200	120	1.12×10^{-2}
761	6.3×10^{-7}	31	4.3	1523	10800	8.36×10^{-2}
766	9.8×10^{-7}	46	3.3	235	60	7.97×10^{-2}
841	4.2×10^{-6}	66	5.0	1020	240	2.67×10^{-2}
842	5.2×10^{-7}	57	4.1	460	120	1.87×10^{-1}
851	1.6×10^{-5}	174	4.9	1440	300	1.85×10^{-2}
879	6.7×10^{-6}	47	4.5	80	42	1.19×10^{-2}
1210	4.2×10^{-5}	526	4.6	795	570	2.13×10^{-2}
1215	5.4×10^{-6}	36	6.2	440	84	1.13×10^{-2}
1220	9.3×10^{-6}	130	3.8	505	240	2.38×10^{-2}
1266	8.4×10^{-7}	39	3.7	105	36	7.89×10^{-2}
1372	9.0×10^{-7}	31	4.1	35	24	5.85×10^{-2}
1424	5.8×10^{-7}	35	5.5	205	168	1.03×10^{-1}
1466	1.3×10^{-5}	249	4.4	940	> 60	3.26×10^{-2}
1504	2.1×10^{-6}	77	4.8	960	288	6.24×10^{-2}
1533	7.0×10^{-6}	214	3.7	230	192	5.20×10^{-2}
1534	3.2×10^{-5}	3420	3.9	350	288	1.82×10^{-1}
1541	2.9×10^{-6}	36	9.4	2700	8844	2.11×10^{-2}
1559	4.2×10^{-6}	50	10.2	1240	714	2.02×10^{-2}
1563	2.9×10^{-4}	2490	4.8	661	858	1.46×10^{-2}
1565	4.8×10^{-7}	18	8.0	1745	1380	6.38×10^{-2}
1624	4.0×10^{-6}	61	5.4	280	192	2.60×10^{-2}
1636	1.0×10^{-6}	37	8.1	320	120	6.29×10^{-2}
1656	1.9×10^{-6}	55	6.3	965	300	4.91×10^{-2}
1696	3.5×10^{-6}	168	6.0	930	546	8.16×10^{-2}
1895	1.2×10^{-6}	25	3.7	135	48	3.54×10^{-2}
2061	2.2×10^{-6}	33	2.9	365	90	2.55×10^{-2}
2104	2.6×10^{-6}	779	3.9	2810	1368	5.10×10^{-1}
2293	3.2×10^{-5}	2065	3.5	3140	3480	1.10×10^{-1}
2628	1.0×10^{-5}	294	4.7	5700	1440	5.00×10^{-2}
2662	9.9×10^{-6}	> 660	3.7	7205	1800	1.13×10^{-1}
3485	1.9×10^{-5}	1920	3.3	455	720	1.72×10^{-1}
3503	6.5×10^{-7}	53	4.1	95	120	1.39×10^{-1}

References

- Bekefi, G. 1966, *Radiation Processes in Plasmas*, (New York: Wiley).
- Brown, J.C. 1971, *Solar Phys.*, **18**, 489.
- Brown, J.C. 1974, *IAU symposium 57, Coronal Disturbances*, ed. G.A. Newkirk (Dordrecht: Reidel), p. 395.
- Cornell, M., Hurford, G., Kiplinger, A., Dennis, B. 1984, *Ap.J.*, **279**, 875.
- Dennis, B.R., Orwig, L.E., Kiplinger, A.L., Gibson, B.R., Kennard, G.S., and Tolbert, A.K. 1985, *The Hard X-ray Burst Spectrometer Event Listing 1980 - 1985*, Technical Memorandum 86236, GSFC.
- Dulk, G. and Dennis, B. 1982, *Ap.J.*, **260**, 875.
- Dulk, G. and Marsh, K. 1982, *Ap.J.*, **259**, 350.
- Gary, D. 1985, *Ap.J.*, **297**, 799.
- Gary, D. and Tang, F. 1984, *Ap.J.*, **288**, 385.
- Holt, S. and Ramaty, R. 1969. *Solar Phys.*, **8**, 119.
- Kai K. 1986, *Solar Phys.*, **104**, 235.
- Kai, K., Kosugi, T., and Nitta, N. 1984, *Publ. Astron. Soc. Japan*, **37**, 155.
- Kosugi, T. and Shiomi, Y. 1983, *Solar Radio Activities Recorded by the Nobeyama Solar Radio observatory in 1978 - 1982*, (Nagano, Japan).
- Lin, R.P. and Hudson, H.S. 1976, *Solar Phys.*, **50**, 153.
- Lu, E. and Petrosian, V. 1988, *Ap.J.*, **327**, 405.
- Leach, J. and Petrosian, V. 1981, *Ap.J.*, **251**, 781.
- Peterson, L. and Winckler J. 1959, *J.G.R.*, **64**, 697.
- Petrosian V. 1973, *Ap.J.*, **186**, 291.
- Petrosian V. 1981, *Ap.J.*, **251**, 727.
- Schmahl, E., Kundu, M., and Dennis, B. 1985, *Ap.J.*, **299**, 1017.
- Takakura, T. and Kai, K. 1966, *Publ. Astron. Soc. Japan*, **18**, 57.
- Vestrand, W.T., Forrest, D.J., Chupp, E.L., Rieger, E., and Share, G.H., 1987, *Ap.J.*, **322**, 1010.

Figure Captions

Figure 1

The ratio of the analytic emissivity equation (17) at $\nu=17\text{GHz}$ and at a viewing angle of $\theta = 60^\circ$ to the numerically calculated emissivity equation (P.8) for $B=350, 500$, and 650 G (dash-dot lines). Also for comparison purposes the ratio of the empirical expression of Dulk and Marsh (1982) to (P.8) is also plotted (dashed lines). For clarity, the curves for $B=500\text{ G}$ and 350 G have been shifted upwards by factors of 10 and 100 respectively.

Figure 2

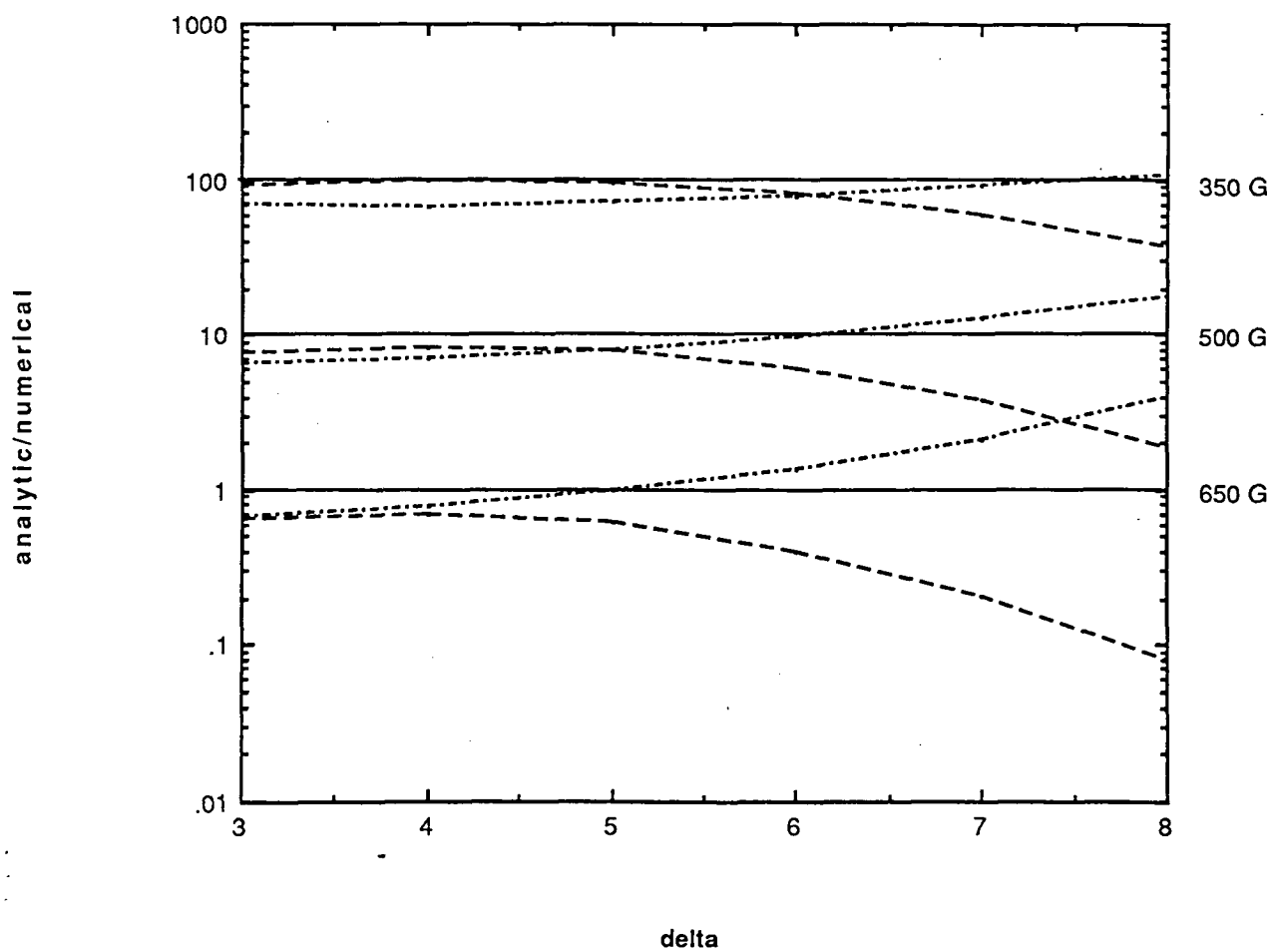
The microwave to X-ray ratio R versus X-ray spectral index γ for the observed flares from Table 1 (squares) and theoretical curves (solid lines) for the thick target model, equation (18). The loop length $L = 2 \times 10^9\text{ cm}$, $\bar{\mu} = 0.5$, and the viewing angle $\theta = 70^\circ$. The four curves are for $B=650, 550, 450$, and 350 G , from top to bottom. For comparison we also plot R (dashed lines) for the same parameters where we have numerically integrated (P.8) for the distribution in equation (7).

Figure 3

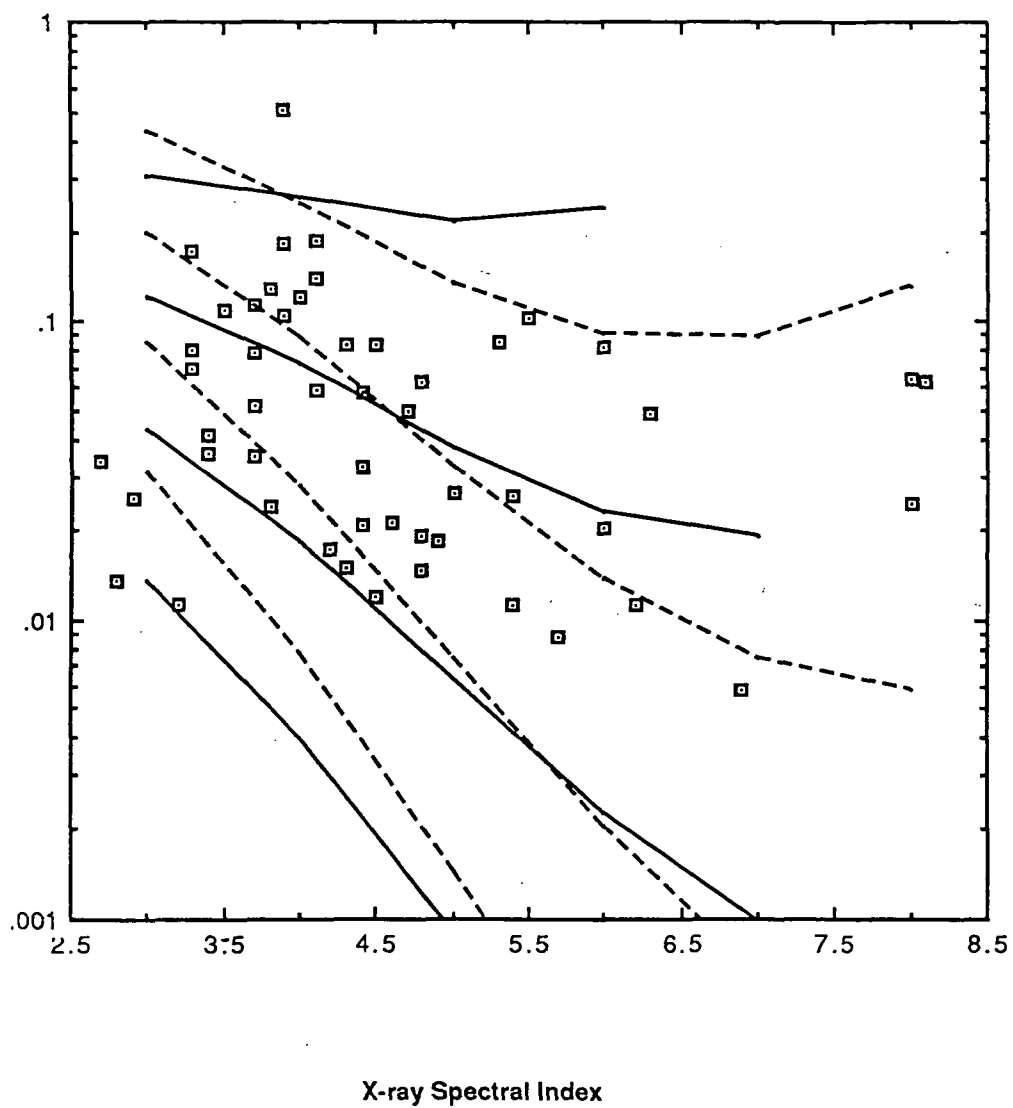
Same as figure 2 for the isotropic thin target model, equation (18). The density $n_0 = 10^{11}\text{ cm}^{-3}$ and $\theta = 70^\circ$. The curves are for $B=450, 350, 250, 150$, and 50 G , from top to bottom.

Figure 4

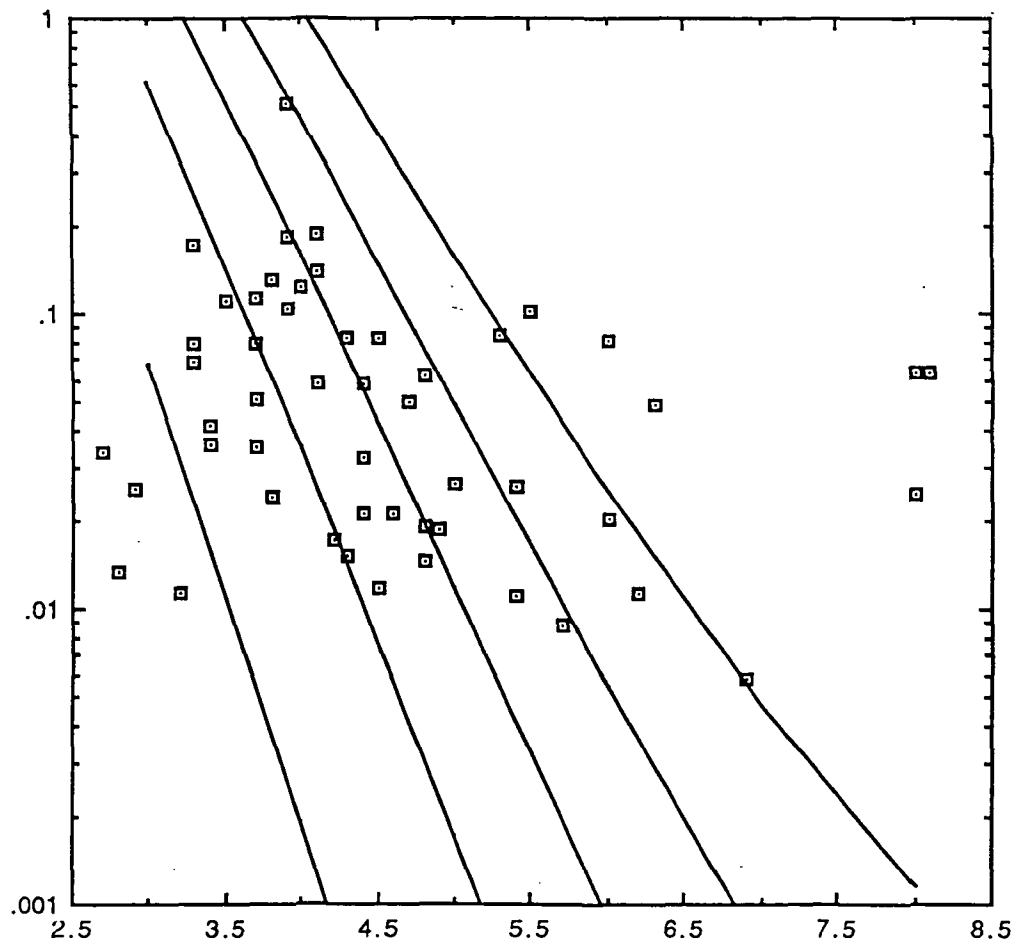
Same as figure 2 for the multithermal constant pressure model, equation (18). The parameter $n_0 = 3.44 \times 10^{10}\text{ cm}^{-3}$, corresponding to the product of density and temperature $nT = 10^{19}\text{ cm}^{-3}\text{ }^\circ\text{K}$ or a constant pressure of $1.38 \times 10^3\text{ dynes cm}^{-2}$. The viewing angle $\theta = 70^\circ$. The curves are for $400, 250, 150$, and 50 G , from top to bottom.



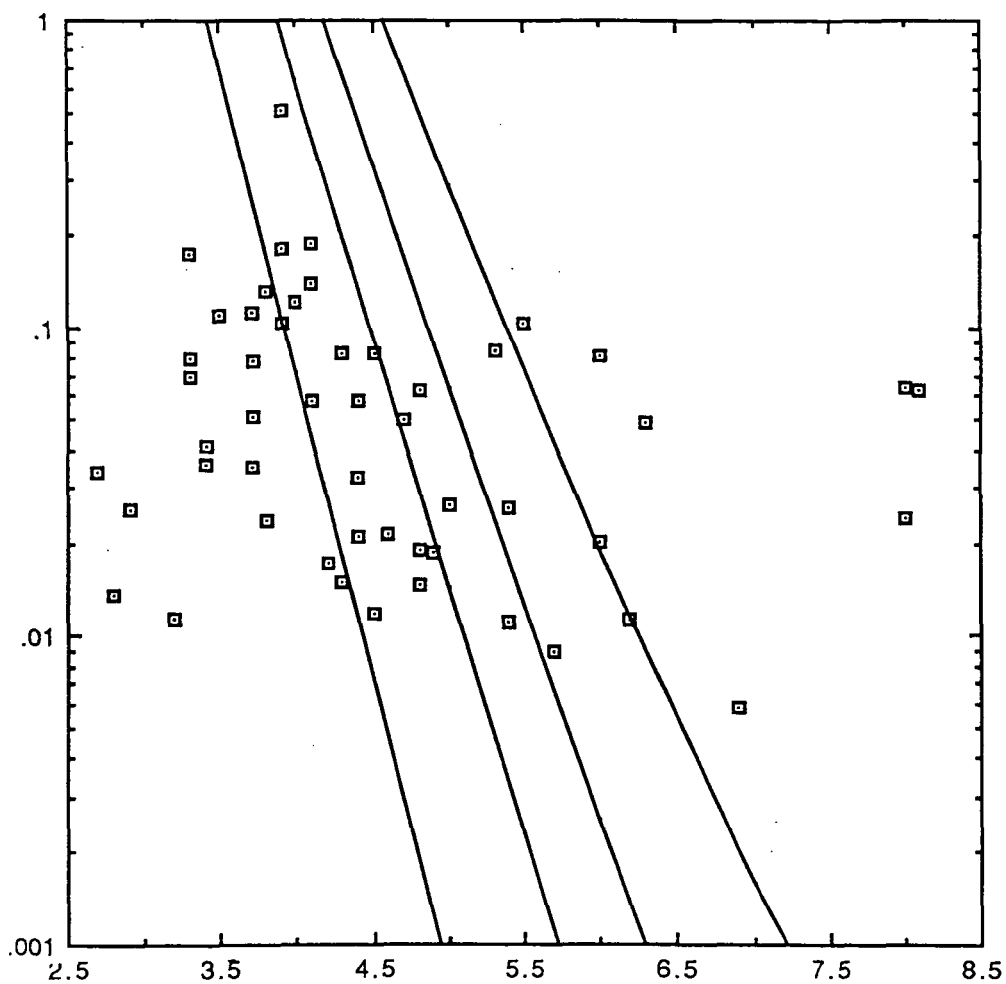
Microwave to X-ray Ratio - R



Microwave to X-ray Ratio - R



Microwave to X-ray Ratio - R



X-ray Spectral Index

Addresses

Edward T. Lu: Center for Space Science and Astrophysics, ERL 323, Stanford University,
Stanford, CA 94305.

Vahé Petrosian: Center for Space Science and Astrophysics, ERL 304, Stanford University,
Stanford, CA 94305.

CENTER FOR SPACE SCIENCE AND ASTROPHYSICS
Electronics Research Laboratory
Stanford University
Stanford, CA 94305